The ionic conductivity and diffusivity of NASICON-type $LiTi_2(PO_4)_3$ and $Li_3Ti_2(PO_4)_3$ solid electrolytes

Lisbon Maake[1*], *Beauty* Shibiri[1], *Phuti* Ngoepe[1] and *Raesibe* Ledwaba[1]

[1]Materials Modelling Centre, University of Limpopo, Private Bag x1106, Sovenga, 0727, South Africa

Abstract. The NASICON-type solid electrolyte $LiTi_2(PO_4)_3$ has excellent electrochemical stability but limited ionic conductivity, largely governed by lithium-ion diffusion. One effective method to enhance this conductivity is by doping Ti^{4+} sites with trivalent cations like Al^{3+}. This substitution introduces additional lithium ions for charge compensation, resulting in compositions such as $Li_{1.3}Al_{0.3}Ti_{1.7}(PO_4)_3$. The improved ionic conductivity in such doped materials is due to the increased lithium-ion concentration. Herein, molecular dynamics simulations are employed to investigate the diffusion coefficients (D) and ionic conductivity of $LiTi_2(PO_4)_3$ under the isothermal–isostress (NST) ensemble and lithiated $Li_3Ti_2(PO_4)_3$ under the microcanonical (NVE) ensemble over the temperature range of 100 – 3100 K. In $LiTi_2(PO_4)_3$, lithium and oxygen Ds increase significantly above 2200 K, while titanium (Ti) and phosphorus (P) remain relatively stable. In $Li_3Ti_2(PO_4)_3$, oxygen D increases sharply, and lithium D peaks above 1600 K before declining after melting. The D of lithium appears to be influenced by the diffusivity of Ti and P, suggesting the structural framework significantly affects lithium mobility. At room temperature, $LiTi_2(PO_4)_3$ shows a low lithium D (1.14×10^{-11} m²/s) and ionic conductivity (3.09×10^{-5} S/cm), while $Li_3Ti_2(PO_4)_3$ exhibits higher lithium D (2.04×10^{-11} m²/s) and conductivity (2.25×10^{-4} S/cm), highlighting enhanced lithium transport.

1 Introduction

Solid-state electrolytes (SSEs) offer a promising alternative to conventional liquid electrolytes, addressing key challenges such as leakage and flammability [1]. Most solid materials have ionic conductivities that are significantly lower than those of advanced liquid electrolytes (LEs), making them seemingly unsuitable as electrolytes. However, certain solid materials, such as NASICON-type $LiTi_2(PO_4)_3$ and anti-perovskite electrolytes, demonstrate superionic conductivity, placing their diffusion performance on par with LEs [1]. Additionally, SSEs typically offer greater mechanical and chemical stability when in contact with elemental lithium compared to LEs, enabling the potential use of lithium metal anodes to boost battery capacity considerably [1, 2].

1Corresponding author: 201803235@myturf.ul.ac.za

As such, NASICON-type lithium titanium phosphate (LTP) solid electrolytes have attracted significant attention as potential electrolytes for application in solid-state batteries due to their stability and relatively high ionic conductivity compared to other solid electrolytes, such as GARNET-type [3] and sulphide-based [4]. However, despite these advantages, their ionic conductivity remains insufficient for large-scale application, limiting their practical use in battery technologies [2, 5].

Therefore, to better understand and address this limitation, it is imperative to study the lithium-ion transport mechanisms in rhombohedral NASICON-structured $LiTi_2(PO_4)_3$ and $Li_3Ti_2(PO_4)_3$. In the NASICON-type materials such as $LiTi_2(PO_4)_3$, lithium ions typically occupy the M1 sites, and, when in excess, they occupy the M2 sites, resulting in relatively low ionic conductivities of 1×10^{-5} S/cm [6]. In lower symmetry phases such as $R\bar{3}$, the M2 sites split into M3 and M3′ positions, where lithium ions occupy distorted oxygen-coordinated environments. This occupation enhances ionic conductivity [6, 7]. The conductivity improvement is attributed to several factors, such as unit cell expansion, local structural distortion, the appearance of extra lithium at M2 sites, and synthesis conditions [6]. However, the similar effects seen across various trivalent dopants suggest that the enhanced performance primarily arises from the partial occupation of the M1 and M3 sites rather than changes in tunnel size. This also points to the potential for higher ionic mobility at the M2 sites [9]. Moreover, aliovalent doping can further promote the migration of ions into these M3 and M3′ sites, as seen in material like $Li_{1.3}Al_{0.3}Ti_{1.7}(PO_4)_3$, leading to significantly improved conductivity of 5×10^{-3} S/cm [8].

Furthermore, in $LiTi_2(PO_4)_3$, lithium ions primarily occupy node sites and migrate along separate chains, whereas in $Li_3Ti_2(PO_4)_3$, lithium ions at transition sites experience repulsion from surrounding lithium ions, leading to concerted motion along multiple 3D pathways [5, 9]. Theoretical calculations indicate that the larger diffusion bottleneck in $Li_3Ti_2(PO_4)_3$ reduces the activation energy compared to $LiTi_2(PO_4)_3$, contributing to its enhanced transport properties [5]. To further explore the impact of structural modifications on ionic conductivity and diffusion, as well as the effect of temperature on local atomic coordination and its influence on diffusion, this study employs molecular dynamics simulations to model the NASICON-type LTP solid electrolytes. By analysing the transport properties across different temperatures, the research provides valuable insights into the relationship between structure, lithium mobility, and ionic conductivity in these materials.

2 Methodology

Molecular dynamics (MD) simulations serve as an effective approach for exploring atomic-level interactions and structural evolution of materials under varying thermodynamic conditions. In this work, the DL_POLY code [10] was employed to carry out temperature-dependent simulations using two distinct statistical ensembles for the pristine LTP and lithiated LTP. The pristine LTP was simulated under the NVE (microcanonical) ensemble, which contains the number of atoms (N), system volume (V), and total energy (E) constant. The lithiated LTP structure under the NST ensemble holds the constant number of atoms (N), applied stress (S), and system temperature (T). The selection of these ensembles was based on findings from a previous study, which validated and confirmed their suitability for achieving reliable and representative results in these structural systems when compared to the literature [11,12]. The pristine structure exhibited a crystalline-to-amorphous phase transition under the NST ensemble at 2500 K, consistent with a value reported in the literature. Similarly, the lithiated structure underwent a comparable phase transition under the NVE ensemble at 1600 K. In contrast, no phase transformation was observed under the other ensembles [11]. To model the atomic interactions within the $LiTi_2(PO_4)_3$ and $Li_3Ti_2(PO_4)_3$ structures, the Buckingham interatomic potentials were defined as:

$$V(r) = A \exp(-r/\rho) - Cr^{-6} \quad (1)$$

where V(r) denotes the Buckingham potential energy arising from the interaction between ions separated by a distance r, with A, ρ, and C representing the specific parameters that define this potential.

2.1 Potential model

The computations in this work are grounded on the Born model of ionic solids [13], where interactions among Li-Ti-P-O ions are primarily driven by long-range Coulombic attractions, counteracted by short-range repulsive forces that prevent ionic overlap. The used Buckingham potentials were verified using the General Utility Lattice Program (GULP) [14], and they yielded results that are in good agreement with experiments [11]. Furthermore, the conventional unit cell parameters of $LiTi_2(PO_4)_3$ from Aatiq et al. [7] used in the calculations were also verified; and the computed parameters closely matched experimental values, with less than 3% deviation, confirming the accuracy and compatibility of the employed potentials and structure model [11].

2.2 Generation of the LTP models

The pristine $LiTi_2(PO_4)_3$ (LTP) crystallizes in a rhombohedral NASICON-type structure with the space group R-3c. Its conventional unit cell contains 108 atoms, and the lattice parameters are a = b = 8.511 Å, c = 20.843 Å, with α = β = 90°, γ = 120°. In this structure, Ti atoms typically occupy the 12c Wyckoff sites, P atoms the 18e sites, and O atoms are distributed among the 36f and 18e sites. Lithium ions are located at the 6b Wyckoff positions, referred to as M1 sites, which lie along the c-axis and exhibit octahedral coordination. Upon lithiation, additional lithium ions are introduced into the framework to form $Li_3Ti_2(PO_4)_3$, which adopts a lower symmetry with the space group R-3 and a total of 120 atoms. The lattice parameters are a = b = 8.383 Å, c = 22.873 Å, α = β = 90°, γ = 120° . The insertion of additional lithium causes redistribution across both M1 (6b) and M3 (18f) sites. The M3 sites, located in the ab-plane, exhibit trigonal prismatic coordination. Both pristine and lithiated LTP structures have TiO_6 octahedra and PO_4 tetrahedra linked together to form a strong 3D framework. Inside this framework, there are two main types of spaces where lithium ions can stay: M1 sites, which lie along the c-axis and have octahedral shapes, and M3 sites, with a trigonal prismatic shape. The key difference between the two materials is the site that the lithium ions occupy. In $LiTi_2(PO_4)_3$, lithium ions mainly occupy the M1 sites at room temperature, while the $Li_3Ti_2(PO_4)_3$ lithium ions are found on the *ab* plane of the TiO_6 octahedra (M3 sites) [7].

Both unit cells were expanded into larger supercells using the METADISE code [15], resulting in supercells with 6912 atoms for the pristine LTP and 7680 atoms for the lithiated LTP. The pristine supercell comprises 384 lithium, 4608 oxygen, 768 titanium, and 1152 phosphorus atoms. In comparison, the lithiated supercell retains the same number of oxygen, titanium, and phosphorus atoms but includes an additional 768 lithium atoms, reflecting the increment of lithium content. Consequently, three essential DL_POLY input files -CONFIG, CONTROL, and FIELD- were generated using METADISE to model the ground-state crystalline structure [10]. The CONFIG file defines the initial atomic positions and velocities, the CONTROL file specifies simulation settings like timesteps and temperature, and the FIELD file outlines molecular details, including atom types, masses, and force field parameters for accurate interaction modelling.

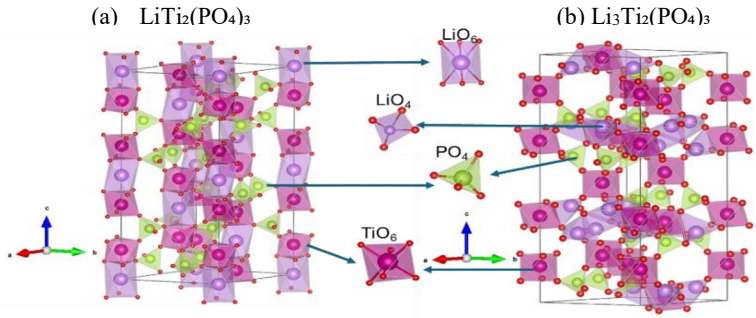

Fig. 1. The conventional unit cells of (a) pristine $LiTi_2(PO_4)_3$ and (b) lithiated $Li_3Ti_2(PO_4)_3$, with NASICON-type frameworks built from TiO_6 octahedra and PO_4 tetrahedra.

2.3 Temperature variation simulation

Temperature variation simulations were performed separately using the NST ensemble for the pristine $LiTi_2(PO_4)_3$ (LTP) and the NVE ensemble for lithiated LTP, after the structural models were generated. In the previously published proceedings paper on pristine LTP, multiple ensembles (NVE, NST, NPT, and NVT) were tested to ensure accurate structure generation and to compare the resulting properties with those reported in the literature. Among these, the NST ensemble yielded results most consistent with the literature, demonstrating a crystalline-to-amorphous phase transition at approximately 2500 K in agreement with reported findings [11]. A similar validation approach was applied to the lithiated LTP. The temperature variation simulations using NPT, NVT, NVE, and NST ensembles were explored. The NVE ensemble, which conserves particle number, volume, and total energy and allows the system to evolve purely under its internal energetic landscape, yielded the most accurate representation. This facilitated the precise observation of intrinsic structural responses driven by lithium-induced strain and excess energy.

The effectiveness of the NVE ensemble in such scenarios is supported by previous studies, which highlight its suitability for investigating non-equilibrium processes, energy redistribution, and phase transitions without artificial damping effects [16]. Under NVE conditions, the lithiated LTP exhibited a clear crystalline-to-amorphous transition around 1600 K, supporting its effectiveness. Consequently, this study reports diffusing coefficients with increasing temperature for the pristine and lithiated LTP using the NST and NVE ensembles, respectively. Simulations were conducted starting from 100 K, with the temperature increased in 300 K intervals up to 3100 K. The Nose-Hoover thermostat was employed due to its known accuracy and efficiency in maintaining constant temperatures during molecular dynamics simulations. The selection of the NST ensemble for pristine $LiTi_2(PO_4)_3$ and the NVE ensemble for lithiated $Li_3Ti_2(PO_4)_3$ was not arbitrary but carefully informed by each system's structural response thermodynamically and phase transition characteristics, ensuring that Li-ion diffusion was evaluated under the most physically representative and ensemble-appropriate conditions.

3 Discussion

3.1 Diffusion coefficients

The pristine and lithiated $LiTi_2(PO_4)_3$ (LTP) supercell structures were successfully generated, and temperature variation calculations were conducted to deduce the diffusion coefficients (D) of the atoms at each temperature, as shown in Fig. 2. For pristine LTP, the D generally increases with temperature. A significant increase in D occurs around 2200 K, corresponding to a structural transition from a crystalline to an amorphous phase; this is driven by an increase in system energy. Lithium ions, which are responsible for ionic conductivity, display relatively higher diffusion coefficients between 100 – 700 K and again above ~2350 K. Furthermore, in the pristine LTP, the diffusion of Ti and P atoms, which form the structural framework, strongly influences the mobility of lithium ions. This is because an increase in titanium (Ti) and phosphorus (P) diffusion correlates with higher lithium-ion diffusion. A similar trend is observed for the lithiated LTP, where the diffusion coefficient of lithium increases alongside that of Ti and P, and decreases when Ti and P diffusion's decreases.

However, from 100 to 400 K, a slight decrease in overall atomic diffusion is observed, although the lithium-ion diffusion coefficient remains higher than that of pristine LTP in this range. This reduction in overall diffusion may be attributed to a decrease in the system's total energy, which, as suggested in the literature, is often associated with an increase in activation energy [11,17]. Moreover, the temperature-induced increase in the overall diffusion coefficient is less pronounced in the lithiated structure compared to pristine LTP. However, within the lithiated system, oxygen atoms exhibit the most significant increase in diffusion relative to other atomic species. Interestingly, at ~2200 K, a slight decrease in Ti and P diffusion coefficients is observed before increasing again at higher temperatures (~2500 K). This behaviour is mirrored and slightly amplified in the lithium-ion diffusion coefficients, as in the pristine structure. This further reinforces the notion that the diffusion coefficients of Ti and P influence lithium-ion diffusion in the material.

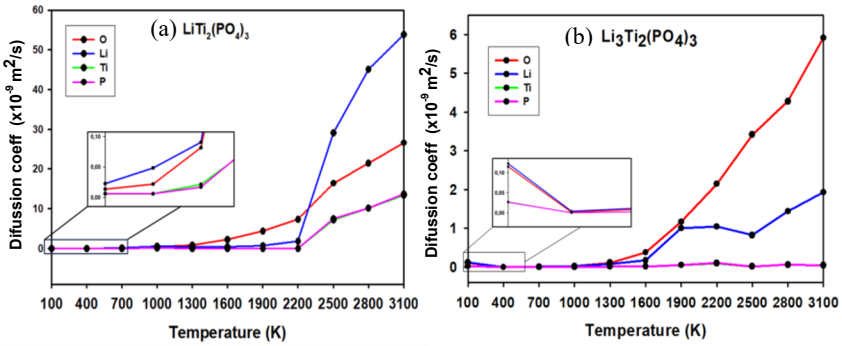

Fig. 2. The diffusion coefficient (D) plots for the (a) pristine and (b) lithiated $LiTi_2(PO_4)_3$ structures.

3.2 Radial distribution functions

To better understand the connection between local atomic structure and ionic transport behaviour, the radial distribution functions (RDF) and their bond lengths are interrogated and depicted in Figures 3 and 4. The RDFs reveal how atoms are spatially arranged around a reference atom, providing valuable insights into both short-range and medium-range structural order [17]. This analysis is essential for interpreting how variations in atomic coordination influence the electrochemical performance of both pristine and lithiated LTP systems. The first peak in the RDF corresponds to the interatomic distance between a specific

pair of atom types, representing their average bond length. The height of this peak indicates the likelihood of finding a neighbouring atom at that particular distance [18].

The framework of NASICON-type $LiTi_2(PO_4)_3$ is composed of TiO_6 octahedra and PO_4 tetrahedra, formed through interactions between Ti, P, and O atoms; therefore, the RDFs of Ti – O and P – O pairs were selected to characterize the structural state of the material, as the stability and connectivity of this framework directly influence the diffusion pathways and mobility of Li^+ ions within the structure [19]. Figure 3 presents the bond lengths of P–O and Ti–O atomic pairs at 300 K for both pristine and lithiated $LiTi_2(PO_4)_3$ structures. In the pristine structure, the average P–O and Ti–O bond lengths are 2.399 Å and 2.546 Å, respectively. Upon lithiation, these bond lengths decrease slightly to 2.390 Å for P–O and 2.451 Å for Ti–O pairs. The slight reduction in average bond lengths following lithiation indicates a mild contraction of the local coordination environment surrounding both phosphorus and titanium atoms, which has the potential to enhance lithium-ion mobility. This contraction is likely driven by structural rearrangements resulting from lithium insertion, particularly as lithium ions migrate to the M2 sites.

Figure 4 presents the radial distribution function (RDF) analyses for pristine and lithiated $LiTi_2(PO_4)_3$ structures, focusing on P–O and Ti–O atomic pairs at 300 K. In both cases, the first prominent peaks for the P–O and Ti–O pairs appear at approximately 2.3 Å. These distances are slightly longer than the typical crystallographic bond lengths, where P–O and Ti–O bonds are usually found near 1.5 Å and 2.0 Å, respectively [19]. The observed elongation may be attributed to structural distortions introduced by nanosizing and lithiation, which are known to broaden and shift RDF peaks due to increased local disorder and bond flexibility [19,20]. Notably, the broader first peak for the P–O pairs, compared to the Ti–O pairs, indicates a wider distribution of interatomic distances for P–O, suggesting greater variability in local bonding environments due to nanoscale distortions and reduced structural symmetry [19].

Additionally, the peak intensities (g(r)) for Ti–O and P–O interactions are noticeably higher in the pristine $LiTi_2(PO_4)_3$ structure than in their lithiated counterpart. A higher peak in the radial distribution function, g(r), corresponds to a greater probability of finding atom pairs at specific interatomic distances, reflecting stronger short-range atomic correlations and a more ordered local environment. Upon lithiation, a notable decrease in the peak heights of g(r) is observed, indicating a reduced probability of well-defined atomic arrangements. This suggests an increase in local structural disorder, likely resulting from lattice distortion induced by lithium insertion. Such disorder disrupts the periodicity of the $LiTi_2(PO_4)_3$ framework and broadens the distribution of interatomic distances. According to Islam et al [20], increased local disorder lowers the energy barriers for Li^+ ion migration by creating a more continuous distribution of accessible hopping sites. Consequently, the lithiation-induced reduction in short-range order enhances the probability of Li^+ diffusion events, leading to improved ionic conductivity. Thus, the RDF results support the hypothesis that lithiation facilitates faster ion transport in $LiTi_2(PO_4)_3$.

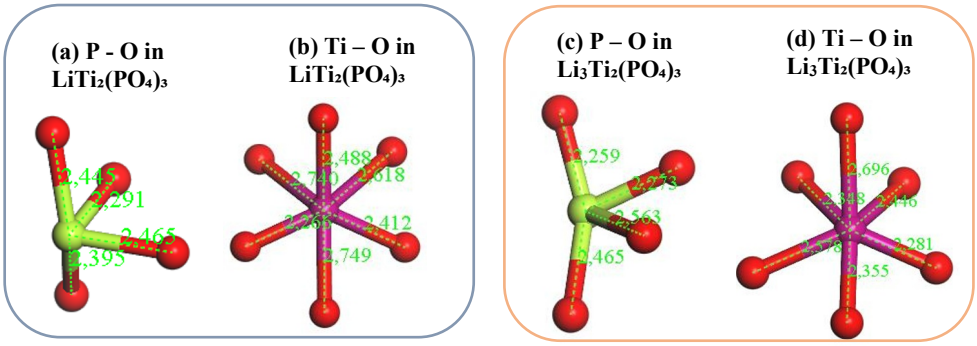

Fig. 3. The bond length distributions for P–O and Ti–O pairs from the $LiTi_2(PO_4)_3$ and $Li_3Ti_2(PO_4)_3$ structures, where (a) and (c) represent P–O bonds, (b) and (d) represent Ti–O bonds in the pristine and lithiated structures, respectively.

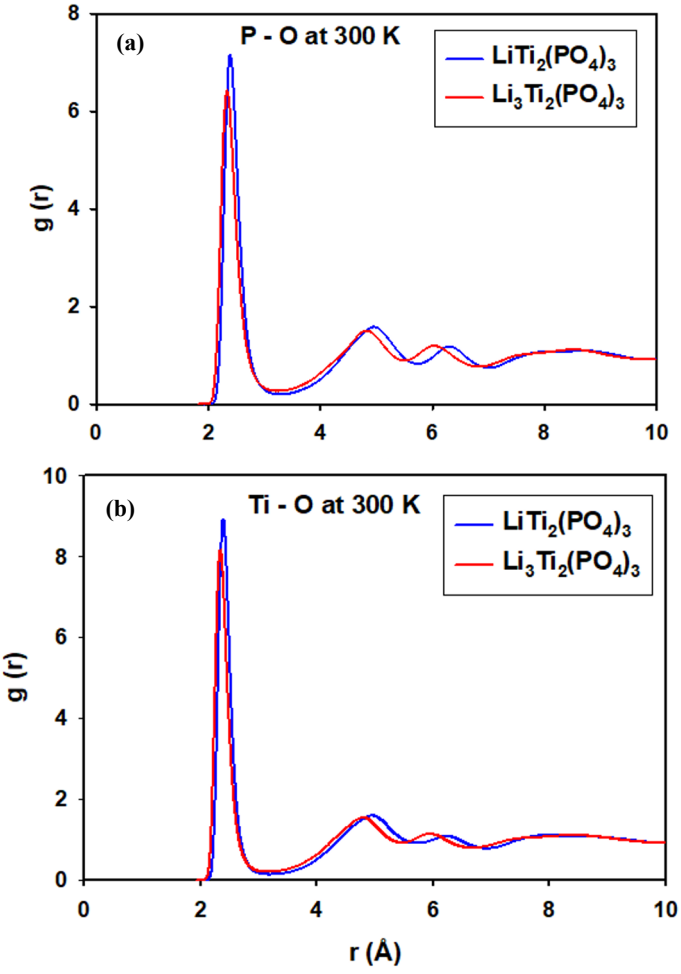

Fig. 4. The radial distribution functions for (a) P-O and (b) Ti-O interactions at 300 K for the pristine and lithiated $LiTi_2(PO_4)_3$ structures simulated under NST and NVE ensembles, respectively.

3.3 Ionic conductivity

To calculate the ionic conductivity of the pristine and lithiated $LiTi_2(PO_4)_3$ structures at room temperature, the study employed the Nernst-Einstein equation:

$$\sigma = \frac{nZ^2e^2D}{K_BT} \quad (2)$$

In this equation, n represents the number density of mobile ions (ions per unit volume, in m^{-3}), the charge number Z corresponds to the valence of the diffusing ion, which is 1 for lithium ions (Li^+), e is the elementary charge, with a constant value equal to 1.602×10^{-19} C, and K_B is the Boltzmann constant with the value of 1.381×10^{-23} J/K. D is the diffusion coefficient, indicating how quickly lithium ions move through the material, measured in m^2/s, and T is the absolute temperature, taken here as 300 K.

The calculated ionic conductivities for the pristine and lithiated $LiTi_2(PO_4)_3$ structures are shown in Table 1 and are compared to the values reported in the literature. The ionic conductivity of the pristine $LiTi_2(PO_4)_3$ was calculated to be 3.09×10^{-5} S/cm, while that of the lithiated $Li_3Ti_2(PO_4)_3$ structure was significantly higher at 2.25×10^{-4} S/cm.

When compared with previously reported values, the pristine structure in this study exhibits an ionic conductivity higher than the literature value of 1.01×10^{-5} S/cm [6]. A similar trend is observed for the lithiated structure, where the conductivity obtained in this study exceeds the previously reported value of 1.90×10^{-4} S/cm from literature [6]. The observed differences in conductivity may be ascribed to the difference in structural scale between the simulations in this work and that from the literature [6]. In this study, solid electrolytes were modelled at the atomic (angstrom) scale, in contrast to the micrometre-scale bulk materials reported in the literature. Previous studies have shown that reducing particle size enhances ionic conductivity, primarily due to increased surface area and shorter diffusion paths [17]. For instance, Dawson et al [21]. demonstrated that using nanoscale modelling techniques increases Li-ion conductivity in LGPS while reducing the particle volume, emphasizing the critical role of nanosizing.

Furthermore, the consistent observation of higher conductivity in both our simulations and previous experimental reports confirms that lithiation of the LTP framework enhances lithium-ion transport. This improvement has been attributed to the increased concentration of mobile lithium ions and the development of more favourable diffusion pathways within the NASICON-type lattice.

Table 1. The comparison between the simulated and experimental ionic conductivities for the pristine and lithiated $LiTi_2(PO_4)_3$ materials [6].

Structures	**Ionic conductivity**	
	This work	**Literature** [6]
$LiTi_2(PO_4)_3$	3.09×10^{-5} S/cm	1.01×10^{-5} S/cm
$Li_3Ti_2(PO_4)_3$	2.25×10^{-4} S/cm	1.90×10^{-4} S/cm

4 Conclusion

The $LiTi_2(PO_4)_3$ and $Li_3Ti_2(PO_4)_3$ materials were investigated for their transport properties as solid electrolytes for Li-ion batteries to shed light on their diffusivity and ionic conductivity. The results show that the lithiated structure ($Li_3Ti_2(PO_4)_3$) exhibits a higher diffusion coefficient than the pristine $LiTi_2(PO_4)_3$, particularly at lower temperatures, indicating enhanced Li^+ mobility. Moreover, radial distribution function analysis at 300 K reveals that the pristine material possesses stronger short-range atomic correlations, whereas

the lithiated structure shows weaker local interactions, which likely contribute to enhanced Li^+ mobility. At room temperature, the calculated ionic conductivity of the lithiated material is significantly higher (2.25×10^{-4} S/cm) than that of the pristine material (3.09×10^{-5} S/cm), consistent with the lithium diffusion of the materials. Furthermore, the simulated ionic conductivities are higher when compared to experimental results. Thus, indeed suggesting that reducing the particle size of LTP enhances Li^+ mobility, thereby improving their ionic conductivity. These findings underscore the potential of $Li_3Ti_2(PO_4)_3$ as a high-performance solid-state electrolyte and highlight lithiation as a viable strategy for boosting ionic conductivity.

The authors acknowledge the Centre for High Performance Computing (CHPC) and the National Integrated Cyberinfrastructure System (NICIS) in Cape Town for computing resources.

The authors declare that the raw data of the findings supporting this study is available.

The National Research Foundation (NRF) Grant number (AHPMDS240916269093) funded this research.

References

1. L. Fan, S. Wei, S. Li, Q. Li, Y. Lu, Recent progress of the solid-state electrolytes for high-energy metal-based batteries. Adv. Energy Mate. **8,** 1702657 (2018)
2. D. Pfalzgraf, D. Mutter, D.F. Urban, Atomistic analysis of Li migration in $Li_{1+x}Al_xTi_{2-x}(PO_4)_3$ (LATP) solid electrolytes. Solid State Ion. **359**, 115521 (2021)
3. Y. Wang, A. Huq, W. Lai, Insight into lithium distribution in lithium-stuffed garnet oxides through neutron diffraction and atomistic simulation: $Li_{7-x}La_3Zr_{2-x}Ta_xO_{12}$ (x = 0 – 2) series. Solid state ion. **255,** 39 (2014)
4 . K.J. Kim, M. Balaish, M. Wadaguchi, L. Kong, J.L. Rupp, Solid-state Li–metal batteries: challenges and horizons of oxide and sulfide solid electrolytes and their interfaces. Adv. Energy Mater. **11**, 2002689 (2021)
5. K. Takada, M. Tominaga, I. Yamada, T. Ichikawa, A. Kato, M. Kondo, S. Kondo, M. Watanabe, Lithium-ion conduction in $LiTi_2(PO_4)_3$. Solid State Ionics, **139**, 241 (2001)
6. X Zhang, D Butenko, L Gao, X Ye, B Hong, S Han, W Xia, S Wang, Y Sun, Y Zhao, J Zhu, Synergistic ion diffusion in lithium titanium phosphate conductors: a tale from solo to ensemble. Chem. Mater. **35**, 4541 (2023)
7. A. Aatiq, M. Ménétrier, L. Croguennec, E. Suard, C. Delmas, On the structure of $Li_3Ti_2(PO_4)_3$. J. Mater. Chem. A. **12**, 2971 (2002)
8. A. Mertens, S. Yu, N. Schön, D.C. Gunduz, H. Tempel, R. Schierholz, F. Hausen, H. Kungl, J. Granwehr, R.A. Eichel, Superionic bulk conductivity in $Li_{1.3}Al_{0.3}Ti_{1.7}(PO_4)_3$ solid electrolyte. Solid State Ionics. **309**, 180 (2017)
9. W. Zhao, J. Yi, P. He, H. Zhou, Solid-state electrolytes for lithium-ion batteries: fundamentals, challenges and perspectives. EER. **2**, 574 (2019)
10. W. Smith, T.R. Forester, DL_POLY_2. 0: A general-purpose parallel molecular dynamics simulation package. J. Mol. Graph. **14**, 136 (1996)
11. L. Maake, B. Shibiri, P. Ngoepe, R. Ledwaba, Analysing phase change of $LiTi_2(PO_4)_3$ solid electrolyte material due to temperature variation. In MATEC Web of Conferences. **406**, 06006 (2024)
12. H. Zheng, E. Sivonxay, M. Gallant, Z. Luo, M. McDermott, P. Huck, K.A. Persson, "The Materials Project," MPContribs Explorer, [online]. Available: https://next-gen.materialsproject.org/contribs/contributions/65a5979f4cd71229efef6895.

13. C.R.A. Catlow, M. Dixon, W.C. Mackrod, Interionic potentials in ionic solids. Comp. Sim. Sol. **130** (2005)
14. J. Gale, GULP: A computer program for the symmetry-adapted simulation of solids. J. Chem. Soc. Faraday Tran. **93**, 629 (1997)
15. G.W. Watson, E.T. Kelsey, N.H. de Leeuw, D.J. Harris, Atomistic simulation of dislocations, surfaces and interfaces in MgO. J. Chem. SOC. **92**, 433 (1996)
16. V. Ponce, D.E. Galvez-Aranda, J.M. Seminario, Analysis of an all-solid-state nanobattery using molecular dynamics simulations under an external electric field. PCCP. **23**, 597 (2021)
17. M.W. Terban, S.J. Billinge, Structural analysis of molecular materials using the pair distribution function. Chem. Rev. **122**, 1208 (2021)
18. D. Hlungwani, R.S. Ledwaba, P. Ngoepe, Simulated synthesis and atomic-level structural characterization of LiNi2O4. In MATEC Web of Conferences. **388**, 07010 (2023)
19. H. Yang, N. Wu, Ionic conductivity and ion transport mechanisms of solid-state lithium-ion battery electrolytes: A review. Energy sci. Eng. **10**, 1643, (2022).
20. M.S. Islam, C.A. Fisher, Lithium and sodium battery cathode materials: computational insights into voltage, diffusion, and nanostructural properties. Chem. Soc. Rev. **43**, 185 (2014)
21. J.A. Dawson, M.S. Islam, 2022. A nanoscale design approach for enhancing the Li-ion conductivity of the $Li_{10}GeP_2S_{12}$ solid electrolyte. ACS Mater. Lett. **4**, 424 (2022)